Three-dimensional urban thermal effect across a large city cluster during an extreme heat wave: observational analysis

Article

Accepted Version

www.reading.ac.uk/centaur

CentAUR

Central Archive at the University of Reading

Reading's research outputs online

The Three-dimensional Urban Thermal Effect across a Large City Cluster during an Extreme Heat Wave: Observational Analysis

Yue MA[1,2], Ping LIANG[1*], Sue GRIMMOND[3], Xuchao YANG[4] Jun LÜ[5], Yihui DING[6]

1 Key Laboratory of Cities' Mitigation and Adaptation to Climate Change in Shanghai, Shanghai Regional Climate Center, CMA, Shanghai 200030, China

2 Shanghai Jiading District Meteorological Bureau, CMA, Shanghai 201800, China

3 Department of Meteorology, University of Reading, Reading RG6 6ET, United Kingdom

4 Ocean College, Zhejiang University, Zhoushan 3160218, China

5 Jiangsu Meteorological Information Center, Jiangsu Meteorological Bureau, Nanjing 210008, China

6 National Climate Center, Beijing 100081, China

*Corresponding author: liangping1107@163.com   Tel: 021-54896543; 18918206543

ABSTRACT

Given extensive and rapid urbanization globally, regional urban thermal effects (UTE) in both canopy and boundary layers under extreme heatwave conditions are of significant interest. Rapid population and economic growth in the Yangtze River Delta (YRD) have created one of the largest city clusters in China. Here we explore the 3-dimensional (3D) UTE in the YRD using numerous observations (high-resolution automatic weather stations, radiosondes, eddy covariance sensors) during the record-setting heat wave (HW) of July-August 2013. Within this HW period, the regional canopy layer UTE is up to 0.6-1.2 °C, with the nocturnal UTE (0.7-1.6 °C) larger than daytime UTE (0.2-0.5 °C). The regional canopy layer UTE is enhanced and expanded northwards   with some rural sites are contaminated by urban influences, especially at night. In the boundary layer, the strengthened regional UTE extends vertically to at least 925 hPa (~750 m) during this HW. The strengthened 3D UTE in the YRD is associated with an enlarged Bowen ratio difference between urban and non-urban areas. These findings about the 3D UTE are important in understanding the thermal environment of urban city clusters in HW and assessing adaption and mitigation strategies.

Keywords: urban thermal effects, 3-dimension, Yangtze River Delta, heat wave

1.   Introduction

Human activities alter the material properties and structures of cities worldwide, with direct impacts on the surface energy balance and the overlying boundary layer. Urban areas are often warmer than their surroundings in response to these modifications. With the large and ever-increasing urban population (United Nations, 2018), the urban thermal environment is of great importance to many sectors of society (e.g. public health, traffic, power industry, water resource management). The east coast Yangtze River Delta (YRD, Fig. 1), is now one of the largest economic zones in China following recent decades of rapid economic development , with the densely populated cluster of cities in this region creating a distinctive Z-shape (Fig. 1) (Xie et al., 2007).

The well-known canopy layer urban heat island (CL-UHI) effect is the difference in canopy layer (~2 m) air temperature between the urban area and its surrounding rural area (Stewart, 2011). To be representative careful consideration needs to be directed to the site selected (World Meteorological Organization, 2022). Although the CL-UHI is widely reported for individual cities in the YRD, such as Shanghai (e.g. Zhang et al., 2010a; Cui and Shi, 2012), Nanjing (e.g. Zeng et al., 2009) and Hangzhou (e.g. Chen et al., 2014), the classification of "urban" and "rural" areas for CL-UHI is critical (e.g. Grimmond et al., 1993; Arnfield, 2003; Stewart, 2011). Many rural observations sites, despite being away from an urban area, are impacted by urbanization to some extent (Lowry, 1977; Huang et al. 2019; Zhang et al., 2021). These impacts may differ with synoptic conditions and mesoscale circulations (e.g. land/sea, Miao et al., 2020). Thus the times when the 'rural' reference is 'contaminated' by urban impacts requires detailed analysis of the source area of the observations (e.g. Oke et al., 2017; World Meteorological Organization, 2022), and   can be challenging to identify (Miao et al., 2020; Zhang et al., 2021).

Across the YRD region (219,000 km², Fig. 1), individual city effects merge and compound each other (Shepherd et al., 2014; Huang et al., 2019). This makes the interpretation of the CL-UHI – as a measure of difference between an urban and rural area – very complex to interpret.. The boundary layer UHI (BL-UHI) is affected by the larger spatial extent of the city (horizontally and vertically and is dominated by local to mesoscale processes (Oke, 1976). In this study, unlike previous YRD CL-UHI research, we consider the urban thermal effects (UTE), not in reference to a single rural area outside one city, rather we consider the urban region and its surroundings through both canopy layer (~2 m air temperatures) and boundary layer influences.

While UTE may not pose stress to citizens under normal thermal conditions, these urban thermal effects can aggravate heat stress and cause severe hazards when compounded by stressful heat wave (HW) temperatures (Wang et al., 2021). Many studies have documented CL-UHI intensification during heatwaves, both   in the daytime (e.g. Shanghai - Jiang et al., 2019) and at night (e.g. Beijing, Guangzhou - Jiang et al., 2019; Madison - Schatz et al., 2015; Shanghai - Ao et al., 2019). With urban expansion in the YRD, the urban influences have become evident in climate signals (Du et al., 2007). Enhancing our understanding of the regional UTE in the YRD is important to assess and improve mitigation and adaptation strategies of large city clusters' thermal stress.

In July and August 2013, a record-breaking heat event occurred in central-east China including the YRD. This was a large spatial event of intense heat, which persisted for a long period with   extensive socio-economic impacts (Zhang et al., 2014). Previous studies of this event focus on the attribution of the HW in terms   of large-scale atmosphere circulation (Peng, 2014; Sun, 2014) and climate change (Xia et al., 2016). The influences of human activities and urban areas in the 2013 HW are also detectable. Changes in anthropogenic forcing at both global and urban scales are found to increase the probability of HW events (Ma et al., 2017; Wang et al., 2017). However, the urban thermal effects in both the canopy and boundary layer across large city clusters under the extreme heat wave conditions are still not clear.

The objective of this study is to examine the 3D UTE of the extensively urbanized YRD through analysis of a dense observational network, including both automatic weather stations (Fig. 1), radiosondes (Table 1) and surface flux sensors (section 2). The analysis explores the influences of an extreme heat wave on the YRD UTE in both the canopy layer and boundary layer (section 3).

2.   Data and methodology

2.1 Study Area

The YRD region (219,000 km^2) includes the Shanghai District, Jiangsu and Zhejiang Provinces (Fig. 1). It is home to about 150 million registered residents (National Bureau of Statistics of China, 2018), of whom approximately 70% are urban dwelling (Liao et al., 2015). Cities in this region include Shanghai, Nanjing, Hangzhou, Suzhou, Ningbo, Wuxi, and Changzhou. Population data for Shanghai District, Jiangsu and Zhejiang Provinces (National Bureau of Statistics of China, 2014) combined with impervious and pervious land-cover fraction data (Gong et al., 2019a,b) indicates the extent urbanized   (Fig. 2). There have been large population increases since the 1980s, with a "Z-shape" city cluster becoming apparent between 1993 and 2013 (e.g. Zhang et al., 2010b; Zhong et al., 2017). Both the "Yangtze River Economic Belt" and the "Belt and Road Initiative" (Lu et al., 2018) cross the YRD.
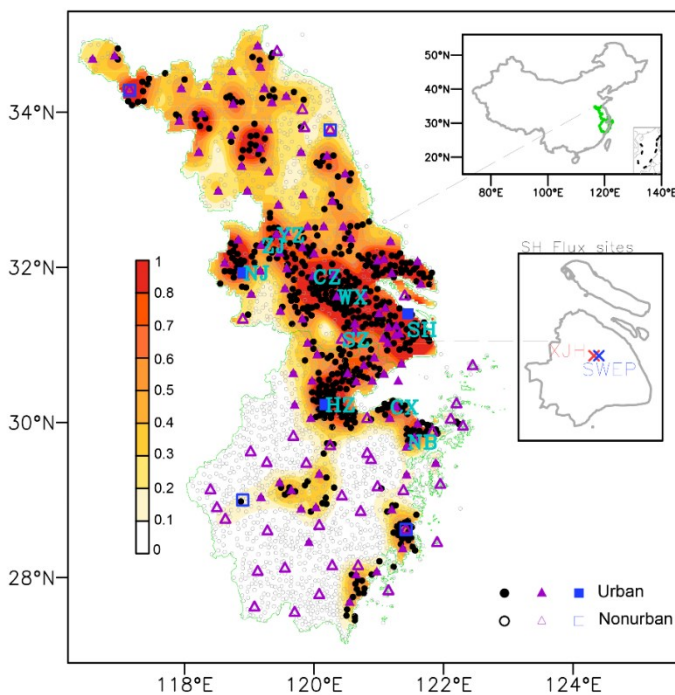

Fig. 1. Location of observations sites and the impervious fraction (shading) in the Yangtze River Delta (YRD) region. The large cities in the 'Z-shaped' city cluster include: Nanjing (NJ), Yangzhou (YZ), Zhenjiang (ZJ), Changzhou (CZ), Wuxi (WX), Suzhou (SZ), Shanghai (SH), Hangzhou (HZ), Cixi (CX), and Ningbo (NB). The automatic weather stations (AWS, circles), national weather sites (NWS, triangles) and radiosonde sites (squares) are classified into urban (solid) and non-urban (hollow). The energy balance observation sites (XJH and SWEP) are in Shanghai (inset). Section 2.2 provides more details.

We use the impervious land cover (Gong et al. 2019a, b) to identify urban stations. These are defined as having an impervious fraction $\geq$ 0.5 in 2013 in their surroundings (circle area: 10 or 100 km2; i.e. radius of 1.785 or 5.642 km). To obtain values for other years, we assume a linear change of $\geq$0.01 annum-1 (Jiang et al., 2020) derived from data for the 1981-2013 period. This follows the method used by others in mainland China (Ren et al., 2011) and United States of America (Hausfather et al., 2013).
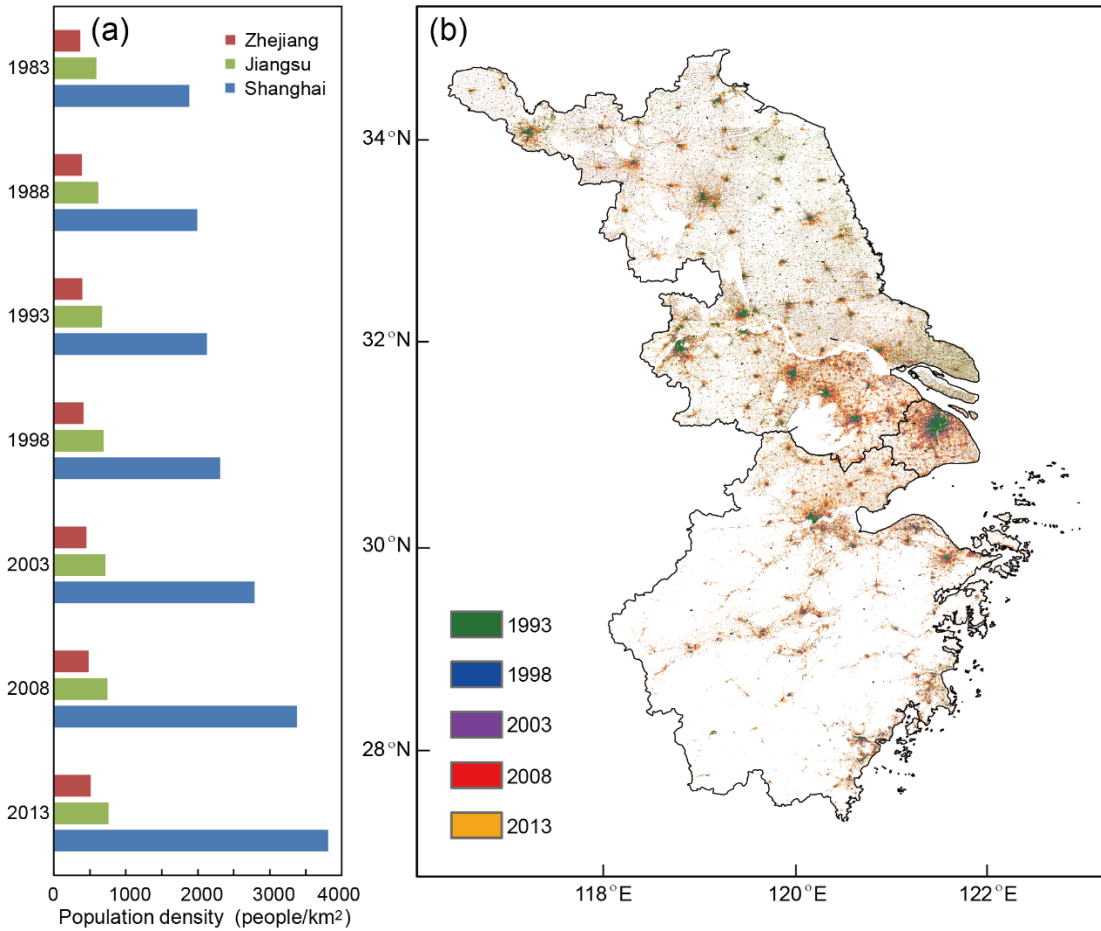
Fig. 2. Urban characteristics through time for Zhejiang Province, Jiangsu Province and Shanghai District: (a) population density (Data: China Statistical Bureau 1983-2013); (b) impervious fraction >0.5 (impervious cover includes building roofs, driveways and parking lots) by the first time period of occurrence (color) (Data: Gong et al. 2019a,b).

2.2 Meteorological Data

In 2013, air temperature (T_{2m}) was measured hourly at 2 m by automatic weather stations (AWS, Vaisala MILOS500, Finland) with a radiation shield (Tan et al., 2015) at 2269 sites (circles, Fig. 1). To reduce topographic site heterogeneity, those located at higher elevations (> 500 m above sea level; Dairaku et al, 2009) are excluded from our analysis.

The AWS sites are flat open areas maintained by the China Meteorological Administration (CMA) regional offices (CMA, 2018). The hourly data are quality-controlled (QC) following World Meteorological Organization (2004) guidelines by the local Meteorological Bureaus of Shanghai District, Jiangsu and Zhejiang provinces. The QC includes checks of consistency (e.g. internal, temporal, spatial) and climatic range. The QC data are used to determine the daily mean, minimum and maximum 2 m air temperature ($T_{mean,2m}$, $T_{min,2m}$ and $T_{max,2m}$, Table 1).

Table 1. Notation used to distinguish the different aspects of the urban thermal effects (UTE)

Height (m agl)	Data source	Mean T_{mean}	Minimum T_{min}	Maximum T_{max}
~2	AWS-MSA	$I_{mean,2A}$	$I_{min,2A}$	$I_{max,2A}$
~2	NWS	$I_{mean,2N}$		
~50-100, 750, 1500, 3000	Radiosonde	$I_{mean,R}$		
	ERA5	$I_{mean,E}$		

The urban or non-urban AWS class assignment (Fig. 1) using impervious fraction (section 2.1) differs little between the two sizes of area (10 and 100 km²) analyzed. Overall, 584 (26%) of the sites are classified as urban. Most of these sites occur near the major city cluster and some smaller cities scattered across northern Jiangsu and southern Zhejiang.

Quality-controlled CMA National Meteorological Information Center daily 2 m air temperature data, observed four times per day (02:00, 08:00, 14:00, 20:00 Beijing standard time, BST), are available from 141 YRD national weather stations (NWS) (e.g. Zhai and Pan, 2003; Ren et al., 2005). Using the same approach for classification as for the AWS sites, 101 are   urban. In this study, we analyze these data for the period 1980-2017 (Table 1).

Within the region, there are seven CMA radiosonde stations (squares, Fig. 1, Table 1). These collect air temperature observations twice a day (08:00 and 20:00 BST) at 11 pressure levels (Guo et al., 2008; Guo and Ding et al., 2009). QC of these data includes assessment of allowable value range and gross errors (http://data.cma.cn/data/cdcdetail/dataCode/B.0011.0001C.html).

As high-resolution L-band radiosonde data (e.g. Jiang et al., 2017; Han et al., 2019) are unavailable in the region, we obtain additional vertical information from ERA5 reanalysis data (Copernicus Climate Change Service, 2017). This data is hourly with 30 km horizontal resolution. Although there is not an urban scheme in the Integrated Forecast System (IFS) reanalysis model, the radiosonde and aircraft data from the region are assimilated.

For both the radiosonde and ERA5 data, four levels (1000, 925, 850, 700 hPa) are analyzed (Table 1), corresponding to about 50-100, 750, 1500 and 3000 m agl (above ground level). To classify the radiosonde data, the impervious fraction within the 100 km^2 circular area around the ground station is used as a proxy for the source area for the sensor as it rises above the surface. Three sites are classified as urban (four non-urban). The urban (non-urban) classification for the 2269 AWS stations is assigned to the ERA5 grid (0.25° x 0.25°).

Shortwave and longwave radiation, turbulent sensible and latent heat fluxes are measured at two sites in Shanghai: (1) commercial – residential area Xujiahui (XJH, 31. 19°N, 121. 43°E), and (2) grass area within the Shanghai World Expo Park (SWEP, 31.19°N, 121.47°E). The measurements at XJH are undertaken at 80 m agl (25 m instrument mast on top of a 55 m building) and at SWEP 1.5 m agl. Sensor details and data processing techniques are the same for both sites (Ao et al., 2016; 2018). The net all-wave radiation ($Q*$), turbulent sensible (Q_H) and latent (Q_E) heat fluxes are directly measured using 10 Hz data to determine 30 min fluxes. However, neither the anthropogenic heat flux (Q_F) nor net storage heat flux (ΔQ_S) are observed. Here, Q_F is not estimated. Although Q_F may increase under HW conditions (Stone, 2012), the Q_F heat emission can be expected to be relatively small (Ichinose et al., 1999) compared to large summertime shortwave radiation. The HW and non-HW day fluxes are compared at both sites using the median fluxes.

2.3 Statistical analysis methods

There are 584 (1685) urban (non-urban) AWS sites available. To reduce the uncertainty from the AWS instrument sites, a regional UTE is calculated using a 'filtering window' that is varied to detect spatial heterogeneities at different spatial scales (Wu and Yang, 2013). To reduce large-scale influences (e.g. of atmospheric circulation, global warming) and urban observation environment impacts, we use very large (radii of 200, 250, 300 km) moving spatial anomaly (MSA) windows around each AWS site relative to canopy layer air temperature source area (order 1 km).

The MSA provides mean temperature classified as urban (T'_u) and non-urban (T'_r). A regional urban-nonurban difference $I_{av}(t)$ is determined for each day (t):

$$I_{av}(t) = \sum_{i=1}^{n_u} \frac{T'_{u,i(t)}}{n_u} - \sum_{j=1}^{n_r} \frac{T'_{r,j(t)}}{n_r}, \qquad (1)$$

using the number of urban (n_u) and non-urban (n_r) sites within the area. Similarly, for each urban site relative to all the nonurban AWS within the area:

$$I_i(t) = T'_{u,i} - \sum_{j=1}^{n_r} \frac{T'_{r,j(t)}}{n_r}. \qquad (2)$$

Positive $I_i(t)$ values indicate a strong UTE. The same techniques are used for both types of canopy layer data (AWS, NWS), but for the radiosonde (R) and ERA5 (E) data MSA is not used (Table 1). As the soundings are sparse of sensors, and the source area for the sensor increases as it rises above the surface, the direct urban-rural differences are used to measure the boundary layer UTE for the R and E data without MSA.

The statistical properties of the daily T_{2m} are assessed using the skewness, kurtosis, interquartile range (IQR), median, and frequency distribution (Mardia, 1970): Skewness measures the asymmetry of the distribution, with positive (negative) skew indicating the presence of a long tail on the high (low) end of the distribution. Kurtosis measures the width of the distribution, with negative (positive) excess kurtosis describing a distribution that is wider (narrower) than the normal distribution. IQR gives the spread between 25th and 75th percentiles values (the median is the 50th percentile). Linear regression using $T_{mean,2m}$ is used to assess the relation between UTE intensity and the HW.

2.4 Heat wave (HW) period

Following Lau and Nath (2012) and Li et al. (2015), HW days are identified using $T_{max,2m}$ and $T_{min,2m}$ thresholds. The CMA operational regulation (Huang et al., 2011) defines high temperatures as daily $T_{max,2m} \geqslant 35°C$ and people's discomfort coming from nocturnal $T_{min,2m} \geq 25°C$ (Zittis et al., 2015). HW days need to meet both criteria (i.e. $T_{max,2m} \geq 35°C$ and $T_{min,2m} \geq 25°C$). Using the areal average of the 2269 YRD AWS, 34 days satisfy $T_{min,2m \geq 25}^{max,2m \geq 35}$ during July-August of 2013.

3. Regional urban thermal effects (UTE) during the heat wave

3.1 The Yangtze River Delta (YRD) 2013 Heat Wave (HW)

In summer 2013, 97.5% of the YRD AWS recorded at least one $T_{max,2m}$ greater than 35°C. At many YRD sites, the summer 2013 temperature observations broke local records (Ma et al., 2017; Wang et al., 2017). Both warm   days (i.e., $T_{max,2m} \geqslant 35$°C) and nights (i.e., $T_{min, 2m} \geqslant 25$°C) were extremely persistent, occurring on more than 40 days over the YRD Z-shaped city cluster in July-August of 2013 (Fig. 3).
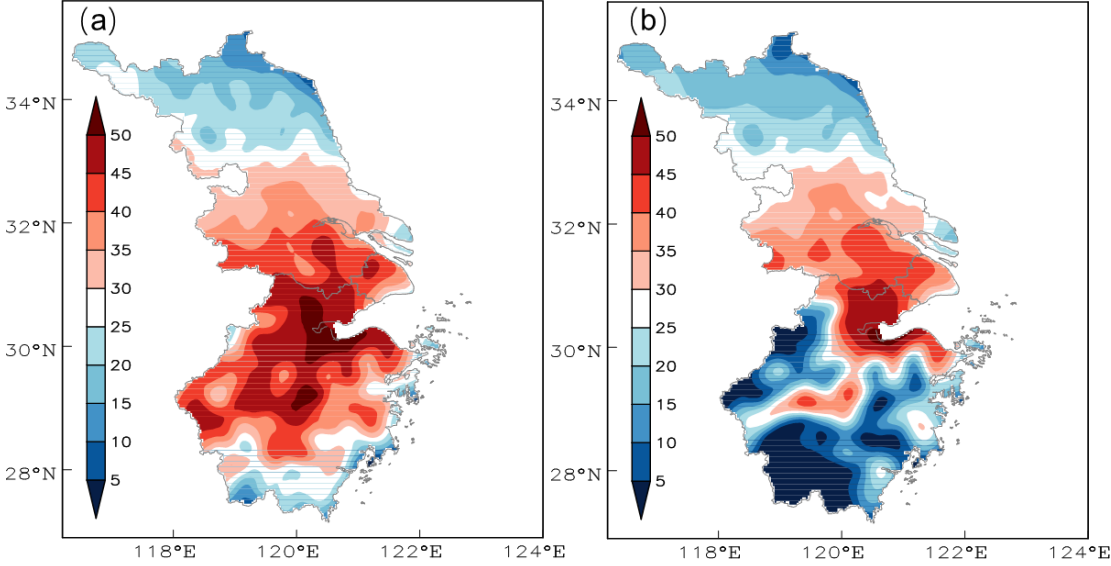

Fig. 3. Number of days in July - August 2013 in the Yangtze River Delta (YRD) when: (a) daily maximum temperature ($T_{max,2m}$) $\geqslant$ 35°C and (b) both daily maximum temperature ($T_{max,2m}$) $\geqslant$35°C and minimum temperature $T_{min,2m} \geqslant$ 25°C from automatic weather station (AWS).

3.2 Canopy layer characteristics of UTE

Analysis of all the AWS air temperature data in the YRD region (section 2.3) shows the city cluster has a negative skewness (-0.63°C; Fig. 4, Table 2). The urban (red, Fig. 4) temperature distribution is shifted to the right of the non-urban (blue, Fig. 4), especially for $T_{min,2m}$ (Fig. 4b), indicating the urban sites are obviously warmer at night. The urban $T_{min,2m}$ and $T_{mean,2m}$ distributions are narrower (i.e. higher kurtosis or closeness to the mean) than the non-urban observations, but differences between urban and non-urban sites for $T_{max,2m}$ are undetectable (Fig. 4c). Thus, the frequency distribution (0.5°C bins) of $T_{min,2m}$ has the expected feature of a regional UTE.
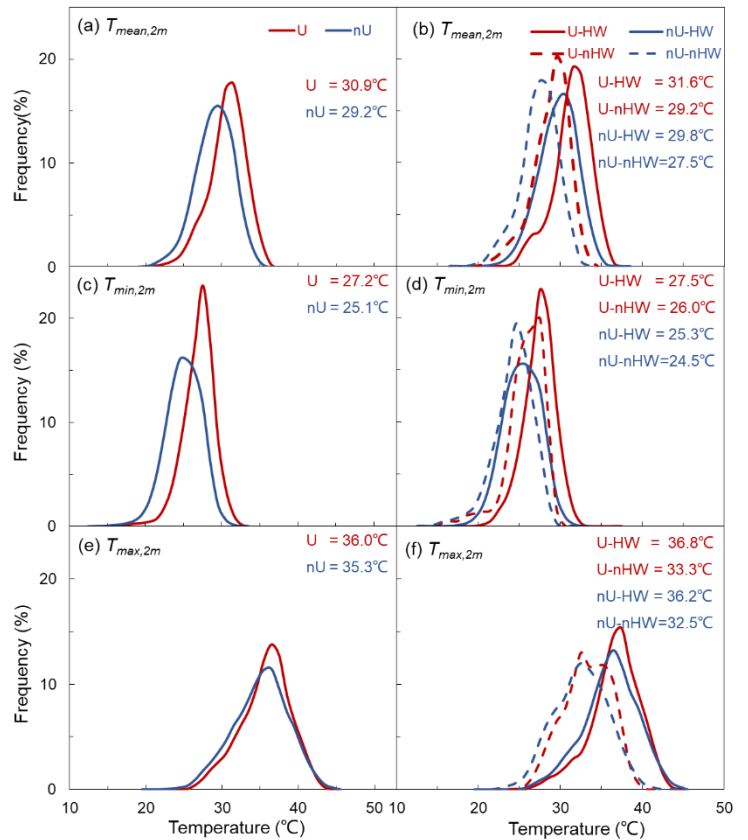

Fig. 4. Frequency distribution (0.5°C bins, %) during July-August 2013 of (a-b) mean ($T_{mean,2m}$, °C), (c, d) minimum ($T_{min,2m}$, °C) and (e, f) maximum ($T_{max,2m}$, °C) temperature at all urban (U, red) and non-urban (nU, blue) automatic weather station (AWS) sites (a, c, e) entire period and (b, d, f) stratified into heat wave (HW, 34 days) and non-HW (nHW, 28 days) conditions. Values given within each plot are the median (°C).

Table 2. Analysis of the frequency curves (Fig. 6) of daily mean temperature ($T_{mean,2m}$, °C), minimum temperature ($T_{min,2m}$, °C) and maximum temperature ($T_{max,2m}$, °C) from automatic weather stations (AWS) under HW and non-HW conditions for urban (U) and non-urban (nU) sites in the Yangtze River Delta (YRD, Fig. 1) during July - August 2013. For statistical methods see section 2.3

| | | $T_{mean,2m}$ (°C) | | $T_{min,2m}$ (°C) | | $T_{max,2m}$ (°C) | |
		U	nU	U	nU	U	nU
July- August	Skewness	-0.59	-0.36	-0.91	-0.37	-0.43	-0.29
	Kurtosis	0.49	0.10	2.47	0.38	-0.10	-0.11
	IQR	3.1	3.4	2.6	3.3	4.2	4.8
	Median	30.9	29.2	27.2	25.2	36.0	35.4
HW	Skewness	-0.63	-0.35	-0.66	-0.19	-0.43	-0.37
	Kurtosis	0.34	-0.01	0.39	-0.17	0.49	0.18
	IQR	2.8	3.2	2.6	3.4	3.6	4.2
	Median	31.6	29.8	27.5	25.4	36.8	36.3
non-HW	Skewness	-0.78	-0.50	-1.37	-0.78	-0.23	-0.10
	Kurtosis	0.67	0.23	2.94	1.08	-0.59	-0.29
	IQR	2.9	3.0	2.7	2.9	4.2	4.7
	Median	29.2	27.5	26.0	24.5	33.3	32.5

In this region during July- August 2013, 34 days meet the HW definition (section 2.4) and 28 not. The expected skew towards higher temperature occurs in both urban and non-urban temperature distribution on HW days (Fig. 4, Table 2), most evident in $T_{min,2m}$. The $T_{min,2m}$ IQR is larger under HW conditions for non-urban than urban sites. There is a pronounced tail toward higher $T_{min,2m}$. The canopy layer UTE is largest for $T_{min,2m}$ (eqn.1, $I_{av,min}$). It varies between 0.7 - 1.6 °C on average for the three radii extents (Fig. 5b). Whereas, $I_{av,mean,2A}$ is slightly less (0.6 -1.2 °C, Fig. 5a) and $I_{av,max,2A}$ the smallest (0.2 - 0.5 °C, Fig. 5c). The large $I_{av,min,2A}$ is consistent with previous studies within the YRD (e.g. Nanjing, Zeng et al. 2009; Shanghai, Cui and Shi, 2012). The $T_{max,2m}$ UTE is much smaller than for $T_{min,2m}$ and $T_{mean,2m}$. Negative UTE $T_{max,2m}$ occur on some days, as observed in traditional studies of urban-rural afternoon temperature differences (e.g. Basara et al., 2008). This is a consequence of lower urban sky view factors. Here negative UTE $T_{max,2m}$ occurs on a few days during the weaker part of the HW (i.e. $T_{max,2m}$ just greater 35 °C) with southeasterly flows from the sea causing, the urban $T_{max,2m}$ to be less than downwind of non-urban areas.
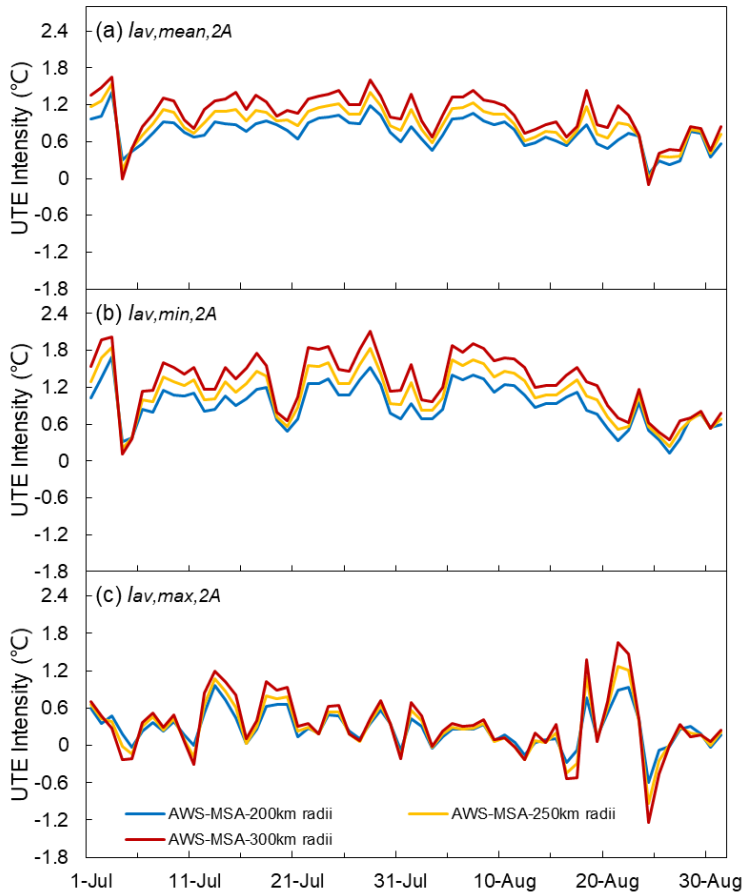

Fig. 5. Daily regional averaged canopy layer urban thermal effects (UTE) ($I_{av,2A}$, eqn. 1, °C) for (a) mean ($T_{mean,2m}$, °C), (b) minimum ($T_{min,2m}$, °C) and (c) maximum ($T_{max,2m}$, °C) temperature from automatic weather station (AWS), using three areal extents (MSA radii (km): 200 (blue), 250 (yellow) and 300 (red)) during July-August 2013 in the Yangtze River Delta (YRD). For methods see Section 2.3.

Both $I_{av,mean,2A}$ (0.2 - 0.3 °C) and $I_{av,min,2A}$ (0.5 - 0.6 °C) are significantly enhanced under HW conditions (significance level $p<0.01$), similar to the enhanced individual city's CL-UHI intensity under the same conditions (Ao et al., 2019; Jiang et al. 2019). However, $I_{av,max,2A}$ does not have a significant change under HW conditions. There are somewhat lower $I_{av,max,2A}$ values during HW conditions than in the non-HW conditions. This feature is like other city clusters in China (e.g. Beijing-Tianjin-Hebei metropolitan region), but the urban effects may be greater in winter than summer in Beijing (Yang et al., 2013).

Analysis of the canopy layer UTE using NWS data $T_{mean,2m}$ ($I_{av,mean,2N}$) for July-August periods from 1980 to 2017, shows that 2013 is the largest (Fig. 6), probably caused by the extensive urbanization over this period and the extreme HW in 2013. The UTE may be enhanced by extreme HWs during midsummer as correlation between UTE and $T_{mean,2m}$ increases to 0.85 from annually averaged 0.76. Linear regression between $I_{av,mean,2N}$ and $T_{mean,2m}$, suggests that the $I_{av,mean,2N}$ is strengthened by 0.2 °C when $T_{mean,2m}$ increases by 1 °C.
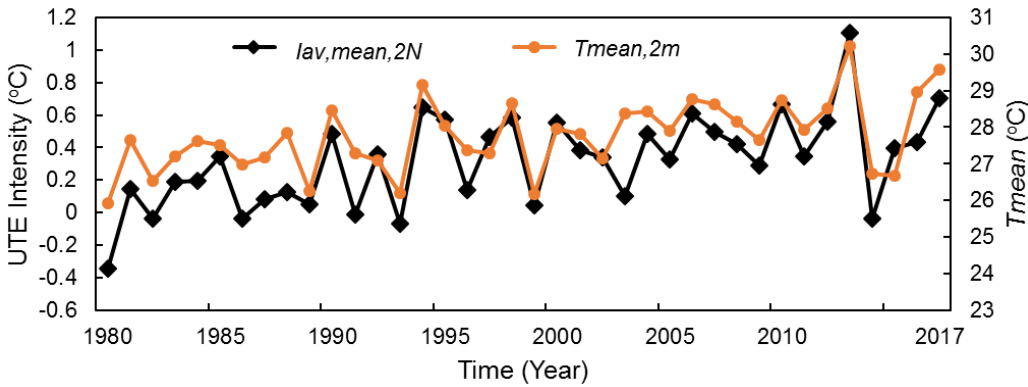

Fig. 6. Interannual (July and August, 1980-2017) variations of average urban thermal effects (UTE) ($I_{av,mean,2N}$, eqn. 1, °C , black) and mean temperature ($T_{mean,2m}$, °C, orange) from national weather stations (NWS, Fig. 1) in the Yangtze River Delta (YRD).

3.3 Regional spatial pattern of UTE at the canopy layer

To examine the canopy layer UTE across the region, MSA is computed for all YRD AWS I_i (eqn. 2, section 2.3). Using a 200 km radius, the results show the positive (warmer) $I_{i,mean,2A}$ and $I_{i,min,2A}$ (Fig. 7a-b) have a Z-shape pattern similar to the YRD urbanization spatial pattern (Fig. 1). Areas with the largest canopy layer UTE (i.e. both $I_{i,mean,2A} >$ 0.5 °C and $I_{i,min,2A} >$ 0.5 °C) cover the Z-shape city cluster and smaller economically developed city groups scattered across Jiangsu and Zhejiang. However, the positive $I_{i,max}$ occurs south of the Z-shape city cluster (i.e. northern Zhejiang, Fig. 7c) with fewer areas above 0.5 °C. This lowers $I_{av,max,2A}$ under HW conditions. The canopy layer UTE extends into nearby non-urban areas under HW conditions for both $I_{i,mean,2A}$ (Fig. 7d) and $I_{i,min,2A}$ (Fig. 7e) > 0.5 °C. The latter area increases the most. During the HW, $I_{i,max,2A}$ intensity is greater than in non-HW conditions (Fig. 7f). Areas where $I_{i,mean,2A}$ and $I_{i,min,2A}$ are > 0.5 °C (Fig. 7d.e) indicate the canopy layer UTE extends to nearby non-urban area under HW conditions, with $I_{i,mean,2A}$ having the largest extension. The canopy layer UTE extension to the nearby non-urban area under HW conditions may result from the combination of individual city's CL-UHI being amplified by the HW (Ao et al., 2019) and the predominately southerly winds (Jiang et al., 2019) advecting the air northwards. Similar canopy layer UTE distributions are found (not shown) using MSA areas with larger radii (e.g. 250 and 300 km).
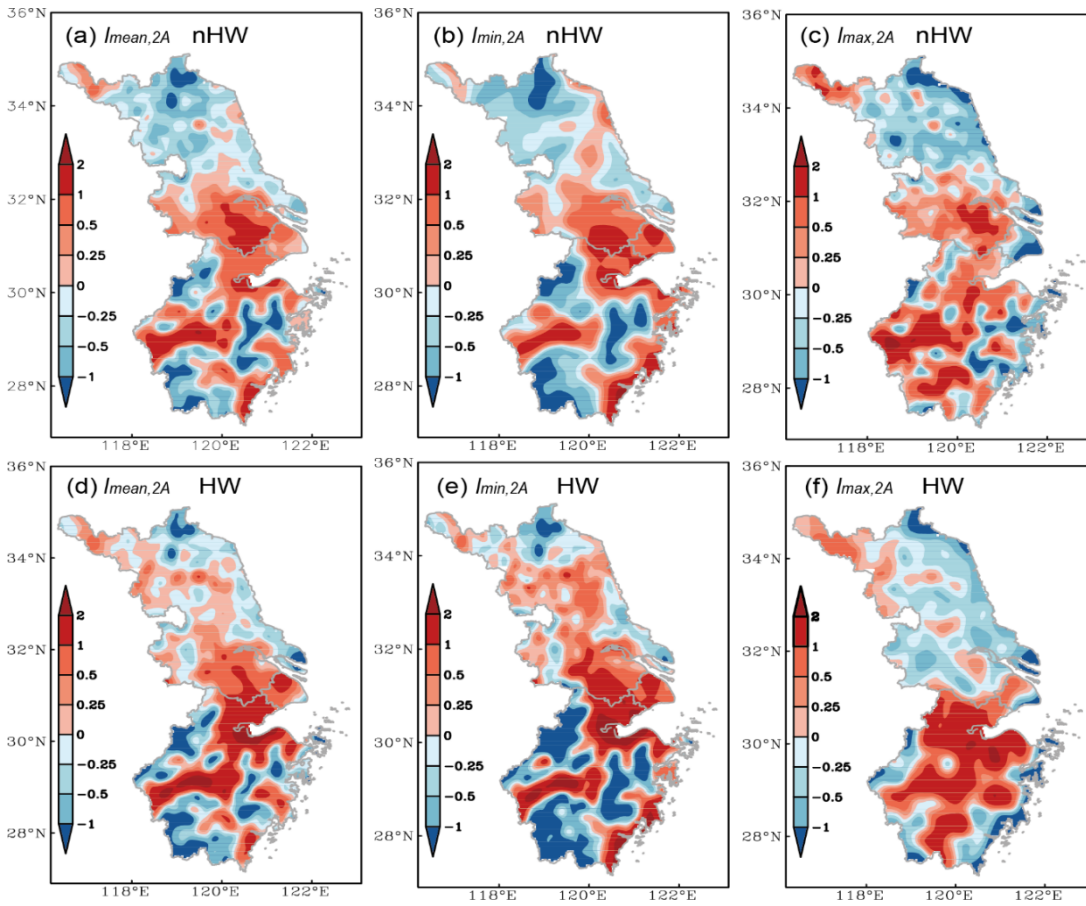
Fig. 7. Spatial variations of average urban thermal effects (UTE) ($I_{i,mean,2A}$, eqn. 2, °C) from automatic weather stations (AWS) using a 200 km radius used during (a-c) non-HW (nHW, 28 days) and (d-f) heat wave (HW, 34 days) conditions for (a, d) mean temperature ($T_{i,mean,2A}$, °C), (b, e) minimum temperature ($T_{i,min,2A}$, °C) and (c, f) maximum temperature ($T_{i,max,2A}$, °C) in the Yangtze River Delta (YRD).

Dominated by the East Asian summer monsoon, southerlies prevail in the YRD lower troposphere during July - August (Tao and Chen, 1987). Wind may advect urban heat from neighboring cities to non-urban areas. For example, high temperature anomalies expanded northwestward in Shanghai and its neighboring cities from 8 to 12 July 2013 (Jiang et al., 2019). Similarly, some non-urban areas in the YRD are influenced by urban heat during both non-HW and HW periods in the summer of 2013 (Fig. 7). By taking the non-urban areas with UTE index larger than 0.5°C as those influenced by urban heat, further calculations shows that about 28% (non-HW) and 35% (HW) of the non-urban areas are affected during two periods. This   suggests (1) some rural sites are contaminated by urban influences in the YRD; (2) the UTE is a more appropriate term than the 'UHI' for discussing urban effects of a large city cluster (such as the YRD); and (3) the quantitative urban influences on non-urban areas differ with synoptic conditions (a topic to be explored in detail in future work).

Consistent with the AWS results, the NWS data shows $I_{i,2N}$ is enhanced during the HW period (not shown). Given that most NWS are urban (section 2.2), the canopy layer UTE amplification at NWS is greater (0.2 - 0.9 °C) than at the AWS during the HW period. The spatial distribution of $I_{i,2N}$ is slightly different from $I_{i,2A}$. A higher canopy layer UTE in the city cluster and a high canopy layer UTE in south of the YRD is evident. However, more (>72%) of the urban NWS are in the south of the YRD. Therefore, the AWS data shows better both the strength and the spatial distribution of canopy layer UTE in the YRD. However, importantly the characteristics of the canopy layer UTE are similar in both the AWS and NWS data.

3.4 Surface energy balance differences associating with UTE

The surface energy balance (SEB) plays a key role in the spatial difference in temperature within and around cities (Oke, 1982; Grimmond et al., 1991), which varies under HW conditions (Li et al., 2015; Sun et al. 2017). The marked differences in energy partitioning between urban and non-urban surfaces are well-documented (e.g., Oke, 1982; Piringer et al., 2002; Oke et al., 2017), with sensible heat flux distinctively larger than the latent heat flux over areas with little vegetation, and increased storage heat fluxes in urban areas (Grimmond and Oke, 1999; Loridan and Grimmond, 2012). As Shanghai is the most urbanized city in the YRD, the surface energy fluxes differences observed here are analyzed in HW and non-HW conditions (Fig. 8).
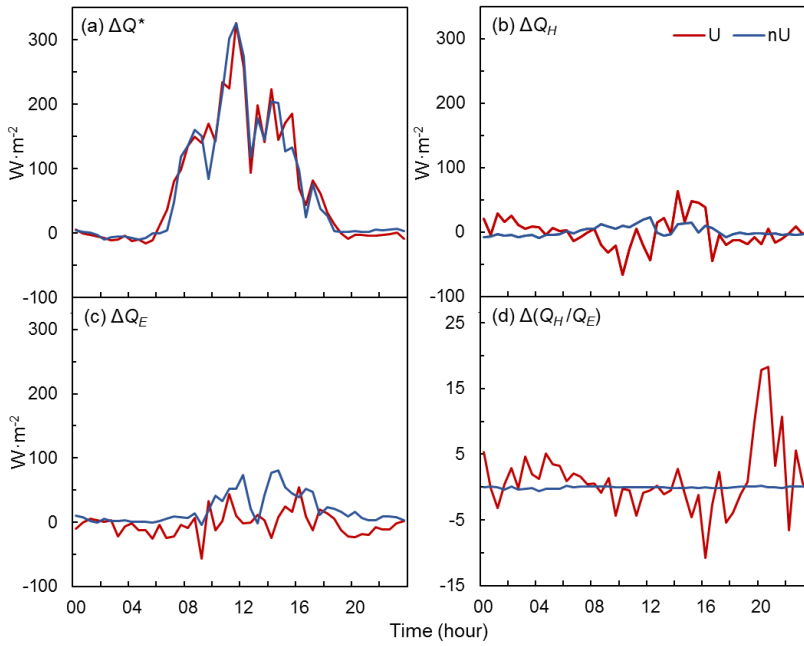
Fig. 8. Diurnal differences (Δ=HW - nHW) in median surface energy balance fluxes: (a) net all wave radiation (Q^*, W·m^{-2}), (b) turbulent sensible heat (Q_H, W·m^{-2}), (c) turbulent latent heat (Q_E, W·m^{-2}) and (d) Bowen ratio (Q_H/Q_E) at an urban (XJH, Fig. 1, 31. 19°N, 121. 43°E, U, red) and a grass (SWEP, 31.19°N, 121.47°E, nU, blue) site. For methods see Section 2.2. Heat wave (HW)= 34 days, non-HW (nHW) =28 days.

Daytime net all-wave radiation (Q^*) is expected to be larger during the HW because of increased solar radiation from clearer skies (Schatz and Kucharik, 2015). The observed total cloud cover is much less during the HW (3.9/10.0) compared to the non-HW (6.6/10.0) at XJH and similarly (HW 4.0/10.0; non-HW 7.0/10.0) at SWEP. At both sites, Q^* increases during the HW (Fig. 8a). However, Q^* is similar between the two nearby sites (11 km separation, Fig. 1) and consistent with urban - nonurban Q^* comparisons (Oke et al., 2017).

The long-persisting HW in the YRD is associated with strong and westward west Pacific subtropical high. Days tend to be cloudless, clear sky enhances the incoming shortwave radiation and therefore increases Q^*, which in turn provides more energy for sensible and latent heat fluxes. As expected, the urban sensible heat flux (Q_H) is positive throughout the day whereas the grass site Q_H is negative at night (20:00 – 06:00, not shown). Under HW conditions, the Q_H increases in the afternoon (13:00 – 16:00) at both flux sites with a larger increase at XJH (~35.0 W m^{-2}) than at the grass site (~1.1 W m^{-2}, Fig. 8b).

The latent heat flux (Q_E) also increases in afternoon - early evening (13:00 – 21:00) at both sites during the HW (Fig. 8c). The median increase at XJH is 1.3 W m^{-2} whereas at the grass site it is 32.1W m^{-2}. The median Bowen ratio (Q_H/Q_E, Fig. 8d) at XJH increased from 6.5 (non-HW) to 8.4 on HW days; but decreased at the grass site from 0.11 (non-HW) to 0.07 (HW). The relatively lower daytime urban Q_E increase allows the enhanced Q_H to warm the urban atmosphere under HW conditions, consistent with HW conditions in London (Ward and Grimmond, 2017). Larger latent heat fluxes (or mass equivalent evaporation) will dry the soil. Unfortunately, we lack soil moisture data to assess this. Reduction in soil moisture is regarded as a principal driver to UTE amplification, but there is a tradeoff between sensible heat and reduced nonurban latent cooling (Fischer et al. 2007), such as seen in the record-breaking 2003 European summer HW.

3.5 Vertical UTE characteristics

The differences in SEB partitioning and canopy layer air temperatures are expected to cause differences in heating of the boundary layer (Zhang et al., 2020). The larger sensible heat flux from the urban surface enhances growth of the urban boundary layer, causing it to develop faster and to a greater height than the non-urban counterpart. Release of large urban storage heat fluxes helps the mixing layer to persist for longer. To explore the vertical characteristics of the UTE both radiosonde and ERA5 data are analyzed (section 2.2).

Radiosonde air temperatures between 1000 and 700 hPa above both urban and nonurban areas are warmer on HW days than non-HW days (Fig.9a,b,d,e, black) with the differences (HW– non-HW) decreasing with height. The vertical $I_{mean,R}$ profiles (Fig.9c, f, black) show the vertical UTE extends to at least 925 hPa (~750 m) but is nearly undetectable at 850 hPa (~1500 m) at both 08:00 and 20:00. The HW days' $I_{mean,R}$ is significantly (level $p<0.05$) warmer than on non-HW days from 1000 to 925 hPa, but above 850 hPa the inverse occurs (i.e., cooler on HW days than non-HW days). Analysis of the ERA5 air temperature has similar vertical profiles to radiosonde air temperatures (Fig.9a,b,d,e, grey). Although $I_{mean,E}$ covers the whole YRD, it is much smaller than $I_{mean,R}$ on both HW and non-HW days, the HW days' $I_{mean,E}$ is significantly (level $p<0.05$) strengthened on HW days from 1000 to 925 hPa at both 08:00 and 20:00 (Fig.9c, f). And it is also undetectable at 850 hPa at both 08:00 and 20:00 as $I_{mean,R}$ showed.
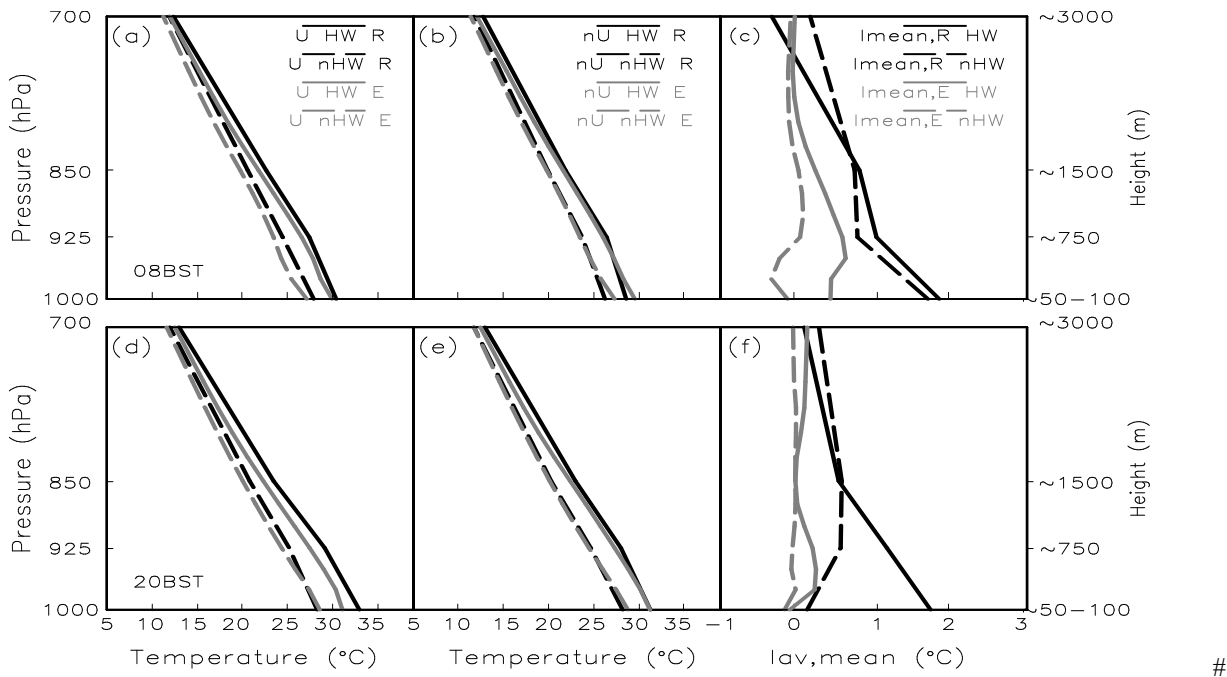
Fig. 9. Vertical profiles of air temperature (°C) and urban thermal effects (UTE) in the Yangtze River Delta (YRD) during July-August 2013 under heat wave (HW, 34 days, solid) and non-HW (nHW, 28 days, dashed) periods from radiosonde (R, black) and ERA5 (E, gray) data for (a, d) urban (U), (b, e) non-urban (nU) and (c, f) U - nU difference ($I_{av,mean}$, eqn. 2, °C) at (a-c) 08:00 and (d-f) 20:00 Beijing standard time (BST). For methods see Section 2.3.

The early evening (20:00) and morning (08:00) vertical UTE decreases with height below 850 hPa under HW conditions (i.e. decreasing urban – nonurban difference with height) as the heat transported from the underlying surface is mixed into an increasing larger volume of air. The subsidence inversion associated with the HW's synoptic scale high pressure inhibits the vertical UTE expanding above 850 hPa.

4.   Final Comments

During the 2013 extreme HW, the canopy layer air temperature distribution in the distinctive Z-shape YRD city-cluster (cf. non-city-cluster) is narrower and skewed towards warmer temperatures, especially at night. The mean canopy layer UTE in the region is up to 0.6-1.2°C, with the nocturnal UTE (0.7-1.6 °C on average) larger than daytime (0.2-0.5 °C on average). During the HW, the nocturnal canopy layer UTE is 0.5-0.6 °C larger than under non-HW conditions. The stronger canopy layer UTE (> 0.5 °C) is mainly located in the Z-shape city cluster but extends beyond under HW conditions. Thus, the HW strengthens the canopy layer UTE and extends horizontally.

During the HW, the difference in Bowen ratios between urban and non-urban areas is enlarged, with both a larger Bowen ratio observed at the urban site and a smaller value over the grass site. The UTE is found to extend vertically to at least 925 hPa (~750 m) or 850 hPa (~1500 m). Unlike canopy layer UHI (CL-UHI) in individual cities dominated by the immediate surroundings, the 3D UTE in large city clusters is affected by the presence of urban area at its lower boundary. In this region with a large city cluster, the effect of the urban area extends in three dimensions (3D; horizontally and vertically) under extreme HW conditions. The regional UTE contaminates surrounding non-urban areas, thus, making the signature of individual cities difficult to measure using the classical urban heat island assumptions (Stewart and Oke, 2012). The methodology proposed in the paper allows the regional UTE to be assessed.

In summary, this study provides insight into the 3D UTE for a large city cluster. Insights gained from the record-setting July-August 2013 HW in YRD and the resulting UTE are important given such conditions are projected   to increase through the mid- to late-21st century. Unlike previous studies, we consider the 3D UTE in both the canopy and boundary layers and enhance our understanding of the effects of urban clusters, especially in the vertical dimension. Utilizing the densest automatic weather station network, allows us to report the UTE variation at high spatial resolution. In terms of future work, hourly and finer (minute) observations (i.e. higher temporal resolution) would be extremely beneficial to improve understanding of the rates of change and the variability (temporal and spatial). Similarly, a wider range of sensors (e.g. L-band radiosondes, doppler radar, thermal profilers) would provide more vertical information. Combined these would enable a better understanding of the 3D influence of large city clusters in a region.

5. References

Ao, X. Y., C. S. B. Grimmond, D. Liu, et al., 2016: Radiation fluxes in a business district of Shanghai, China. *J. Appl. Meteor. Clim.*, **55**, 2451–2468, doi: /10.1175/JAMC-D-16-0082.1.

Ao, X. Y., C. S. B. Grimmond, H. C. Ward., et al., 2018: Evaluation of the Surface Urban Energy and Water balance Scheme (SUEWS) at a dense urban site in Shanghai: Sensitivity to anthropogenic heat and irrigation. *J. Hydro. Meteor.*, **19**, 1983–2005, doi: /10.1175/JHM-D-18-0057.1

Ao, X. Y., J. G. Tan, X. Zhi, et al., 2019: Synergistic interaction between urban heat island and heat waves and its impact factors in Shanghai. *Acta Geogr. Sinica*, **74**, 1789–1802, doi: /10.11821/dlxb201909007.

Arnfield, A. J., 2003: Two decades of urban climate research: A review of turbulence, exchanges of energy and water, and the urban heat island. *Int. J. Climatol.*, **23**, 1–26. doi:/10.1002/joc.859.

Basara, J. B., P. K. Hall, A. J. Schroeder, et al., 2008: Diurnal cycle of the Oklahoma City urban heat island. *J. Geogr. Res.*, **113**, D20109, doi: /10.1029/2008jd010311.

Chen, F., X. C. Yang, and W. P. Zhu, 2014: WRF simulations of urban heat island under hot-weather synoptic conditions: the case study of Hangzhou city, China. *Atmos. Res.*, **138**, 364–377, doi: /10.1016/j.atmosres.2013.12.005.

China Meterological Administration, 2018: Technical Specifications for Maintenance of Regional Automatic Weather Station. QX/T 465–2018.

Copernicus Climate Change Service, 2017: *ERA5:* Fifth generation of ECMWF atmospheric reanalyses of the global climate. Copernicus Climate Change Service Climate Data Store (CDS), https://cds.climate.copernicus.eu/cdsapp#!/home.

Cui, L. L., and Shi, J., 2012: Urbanization and its environmental effects in Shanghai, China. *Urban Climate*, **2**, 1–15, doi: /10.1016/j.uclim.2012.10.008.

Dairaku, K., K. Kuraji, M. Suzuki, et al., 2009: The effect of rainfall duration and intensity on orographic rainfall enhancement in a mountainous area. *J. Japan Soc. hyorol. & Water Resour.*, **13**, 57-68. doi: /10.3178/jjshwr.13.57.

Du, Y., Z. Q. Xie, Y. Zeng, et al., 2007: Impact of urban expansion on regional temperature change in the Yangtze River Delta. *J. Geogr. Sci.*, **17**, 387-398. doi: /10.1007/s11442-007-0387-0.

Gong, P., X. C. Li, and W. Zhang, 2019a: 40-year (1978–2017) human settlement changes in China reflected by impervious surfaces from satellite remote sensing. *Sci. Bull.*, **64**, 756–763, doi: /10.1016/j.scib.2019.04.024.

Gong, P., H. Liu, M. N. Zhang, et al., 2019b: Stable classification with limited sample: Transferring a 30-m resolution sample set collected in 2015 to mapping 10-m resolution global land cover in 2017. *Sci. Bull.*, **64**, 370–373, doi: /10.1016/j.scib.2019.03.002.

Grimmond, C. S. B., H. A. Cleugh, and T. R. Oke, 1991: An objective urban heat storage model and its comparison with other schemes. *Atmos. Environ.*, **25**, 311–326, doi: /10.1016/0957-1272(91)90003-W.

Grimmond, C. S. B., T. R. Oke, and H. A. Cleugh, 1993: The role of "rural" in comparisons of observed suburban- rural flux differences. *Inter. Associ. Hydro. Sci. Publication*, **212**, 165-174.

Grimmond, C. S. B., and T. R. Oke, 1999: Heat Storage in Urban Areas: Local-Scale Observations and Evaluation of a Simple Model. *J. Appl. Meteor.*, **38**, 922–940, doi: /10.1175/1520-0450(1999)038<0922:HSIUAL>2.0.CO;2.

Guo, Y. J., and Y. H. Ding, 2009: Long-term free-atmosphere temperature trends in China derived from homogenized in situ radiosonde temperature series. *J. Climate*, **22**, 1037–1051, doi: /10.1175/2008JCLI2480.1.

Guo, Y. J., P. W. Thorne, M. P. Mccarthy, et al., 2008: Radiosonde temperature trends and their uncertainties over eastern China. *Int. J. Climatol.*, **28**, 1269–1281, doi: /10.1002/joc.1633.

Hausfather, Z., M. J. Menne, C. N. Williams, et al., 2013: Quantifying the effect of urbanization on U.S. Historical Climatology Network temperature records. *J. Geophys. Res. Atmos.*, **118**, 481–494, doi: /10.1029/ 2012JD018509.

Han, Y., Y. W. Zhou, J. P. Guo, et al., 2019: The characteristics of spatial and temporal variations in the PBL during the landfall of tropical cyclones across East China. *J. Appl. Meteor.*, **58**, 1557–1572. 10.1175/JAMC-D-18-0131.1.

Huang, Z., H. Chen, and H. Tian, 2011: Research on the heat wave index. *Meteor. Mon.*, **37**, 345–351, doi: /10.7519/j.issn.1000-0526.2011.03.013. (in Chinese)

Huang, B., G. Ni, and C. S. B. Grimmond, 2019: Impacts of upwind urban expansion on regional climate during heat waves. *Atmosphere*, **10**, 364, doi: /10.3390/atmos10070364.

Ichinose, T., K. Shimodozono, and K. Hanaki, 1999: Impact of anthropogenic heat on urban climate in Tokyo. *Atmos. Environ.*, **33**, 3897–3909, doi: /10.1016/s1352-2310(99)00132-6.

Jiang, X. L., D. H. Wang, J. J. Xu, et al., 2017: Characteristics of observed tropopause height derived from L-band sounder over the Tibetan Plateau and surrounding areas. *Asia-Pacific J. Atmos. Sci.*, **53**, 1–10, doi: /10.1007/s13143-016-0035-7.

Jiang, S. J., X. H. Lee, J. K.Wang, et al., 2019: Amplified urban heat islands during heat wave periods. *J. Geo. Res. Atmos.*, **124**, 7797–7812, doi: /10.1029/2018JD030230.

Jiang, S. J., K. C. Wang, and Y. N. Mao, 2020: Rapid local urbanization around most meteorological stations explains the observed daily asymmetric warming rates across China from 1985 to 2017, *J. Climate*, **33**, 9045-9061. doi: /10.1175/JCLI-D-20-0118.1

Lau, N. C. and M. J. Nath, 2012: A model study of heat waves over North America: meteorological aspects and projections for the twenty-first century. *J. Climate.*, **25**, 4761–4784, doi: /10.1175/JCLI-D-11-00575.1.

Li, D., T. Sun, M. F. Liu, et al., 2015: Contrasting responses of urban and rural surface energy budgets to heat waves explain synergies between urban heat islands and heat waves. *Environ. Res. Lett.*, **10**, 054009, doi: /10.1088/1748-9326/10/5/054009.

Liao, J. B., T. J. Wang, Z. Q. Jiang, et al., 2015: WRF/Chem modeling of the impacts of urban expansion on regional climate and air pollutants in Yangtze River Delta, China. *Atmos. Environ.*, **106**, 204–214, doi: /10.1016/j.atmosenv.2015.01.059.

Lowry, W. P., 1977: Empirical estimation of urban effects on climate: a problem analysis. *J. Appl. Meteor.*, **16**, 129–135, doi: /10.1175/1520-0450(1977)016<0129:EEOUEO>2.0.CO;2.

Loridan, T. and C. S. B. Grimmond, 2012: Characterization of energy flux partitioning in urban environments: links with surface seasonal properties. *J. Appl. Meteor. Climatol.*, **51**, 219–241, doi: /10.1175/JAMC-D-11-038.1.

Lu, H., M. L. Zhang, W. W. Sun, et al., 2018: Expansion analysis of Yangtze River Delta urban agglomeration using DMSP/OLS nighttime light imagery for 1993 to 2012. *ISPRS Int. J. Geo-Inf.*, **7**, 52, doi: /10.3390/ijgi7020052.

Mardia, K. V., 1970: Measures of multivariate skewness and kurtosis with applications. *Biometrika*, **57**, 519–530. doi: /10.1093/biomet/57.3.519.

Ma, S. M., T. J. Zhou, D. A. Stone, et al., 2017: Attribution of the July-August 2013 heat event in Central and Eastern China to anthropogenic greenhouse gas emissions. *Environ. Res. Lett.*, **5**, 054020, doi: /10.1016/10.1088/1748-9326/aa69d2.

Miao, S. G., W. M. Jiang, P. Liang, et al., 2020: Advances in urban meteorological research in China. *J. Meteor. Res.*, **34**, 218–242, doi: 10.1007/s13351-020-9858-3.

National Bureau of Statistics of China, 2014: Statistical Yearbook of the Republic of China 2014. (in Chinese)

National Bureau of Statistics of China, 2018: Statistical Yearbook of the Republic of China 2018. (in Chinese)

Oke, T. R., 1976: The distinction between canopy and boundary‐layer urban heat islands, *Atmosphere*, **14**, 268-277, doi:/10.1080/00046973.1976.9648422.

Oke, T. R., 1982: The energetic basic of the urban heat island. *Q. J. Roy. Meteor. Soc.*, **108**, 1–24, doi: /10.1002/qj.49710845502.

Oke, T. R., G. Mills, A. Christen, et al., 2017: *Urban Climates*. Cambridge University Press, 546 pp.

Peng, J. B., 2014: An investigation of the formation of the heat wave in southern china in summer 2013 and the relevant abnormal subtropical high activities. *Atmos. Oceanic Sci. Lett.*, **7**, 286–290, doi: /10.3878/j.issn.1674-2834.13.0097.

Piringer, M., C. S. B. Grimmond, S. M. Joffre, et al., 2002: Investigating the surface energy balance in urban areas- recent advances and future needs. *Water Air and Soil Poll.*, **2**, 1–16, doi: /10.1007/978-94-010-0312-4_1.

Ren, G. Y., Z. Y. Chu, Y. Q. Zhou, et al., 2005: Recent Progresses in Studies of Regional Temperature Changes in China. *Clim. Environ. Res.*, **10**, 701–717, doi: /v10.1007/s10409-004-0010-x.

Ren, G. Y., Y. H. Ding, and G. L. Tang, 2017: An overview of mainland China temperature change research. *J. Meteor. Res.*, **31**, 3–16, doi: 10.1007/s13351-017-6195-2.

Ren, Y. Y., and G. Y. Ren, 2011: A remote-sensing method of selecting reference stations for evaluating urbanization effect on surface air temperature trends. *J. Climate*, **24**, 3179–3189, doi:/10.1175/2010JCLI3658.1.

Schatz, J., and C. J. Kucharik, 2015: Urban climate effects on extreme temperatures in Madison, Wisconsin, USA. *Environ. Res. Lett.*, **10**, 094024, doi: /10.1088/1748-9326/10/9/094024.

Shepherd, M., T. Andersen, C. Strother, et al., 2014: Urban Climate Archipelagos: A new Framework for urban impacts on climate. Earthzine.

Stewart, I. D., 2011: A systematic review and scientific critique of methodology in modern urban heat island literature. *Inter. J. Climatol.*, **31**, 200-217, doi: /10.1002/joc.2141.

Stewart, I. D., and T. R. Oke, 2012: Local climate zones for urban temperature studies. *Bull. Atmos. Meteor. Soc.*, **93**(12), 1879–1900, doi: /10.1175/bams-d-11-00019.1.

Stone, B., 2012: *The City and the Coming Climate*. Cambridge University Press, 206 pp.

Sun, J., 2014: Record-breaking SST over mid-North Atlantic and extreme high temperature over the Jianghuai–Jiangnan region of China in 2013.*Chinese Sci. Bull.*, **59**, 3465–3470, doi: /10.1007/s11434-014-0425-0.

Sun, T., S. Kotthaus, D. Li, et al., 2017: Attribution and mitigation of heat wave-induced urban heat storage change. *Environ. Res. Lett.*, **12**, 114007, doi: /10.1088/1748-9326/aa922a.

Tan, J. G., L. M. Yang, C. S. B. Grimmond, et al., 2015: Urban integrated meteorological observations: practice and experience in Shanghai, China. *Bull. Amer. Meteoro. Soc.*, **96**(1), 197–210, doi: /10.1175/BAMS-D-13-00216.1.

Tao, S. Y., and L. X. Chen. 1987: *A Review of Recent Research on the East Asian Summer Monsoon in China*. Oxford University Press, New York. 60-92 pp.

United Nations, 2018: 2018 Revision of World Urbanization Prospects. United Nations Department of Economic and Social Affairs. 1–126.

Wang, J., Z. W. Yan, X. W. Quan, et al., 2017: Urban warming in the 2013 summer heat wave in eastern China. *Climate Dyn.*, **48**, 3015–3033, doi: /10.1007/s00382-016-3248-7.

Wang, J., Y. Chen, W. L. Liao, et al., 2021: Anthropogenic emissions and urbanization increase risk of compound hot extremes in cities. **11**, 1084–1089, *Nat. Clim. Chang*, doi:/10.1038/s41558-021-01196-2.

Ward, H. C., and C. S. B. Grimmond, 2017: Assessing the impact of changes in surface cover, human behaviour and climate on energy partitioning across Greater London. *Landscape and Urban Plan.*, **165**, 142–161, doi: /10.1016/j.landurbplan.2017.04.001.

World Meteorological Organization. 2004: Guidelines on Quality Control Procedures for Data from Automatic Weather Stations.

World Meteorological Organization. 2022: Guidance to Measuring, Modelling and Monitoring the Canopy Layer Urban Heat Island.

Wu, K., and X. Q. Yang, 2013: Urbanization and heterogeneous surface warming in eastern China. *Sci. Bull.*, **58**, 1363–1373, doi: /10.1007/s11434-012-5627-8.

Xia, J., K. Tu, Z. W. Yan, et al., 2016: The super-heat wave in eastern China during July-August 2013: a perspective of climate change. *Int. J. Climatol.*, **36**, 1291–1298, doi: /10.1002/joc.4424.

Xie, Z. Q., Y. Du, Y. Zeng, et al., 2007: Impact of urban expansion on regional temperature change in the Yangtze River Delta. *Acta. Geo. Sinica*, **62**, 717–398, doi: /10.1007/s11442-007-0387-0.

Yang, P., G. Y. Ren, and W. D. Liu, 2013: Spatial and temporal characteristics of Beijing urban heat island intensity. *J. Appl. Meteor. Climatol.*, **52**, 1803–1816, doi: /10.1175/JAMC-D-12-0125.1.

Zeng, Y., X. F. Qiu, L. H. Gu, et al., 2009: The urban heat island in Nanjing. *Quatern. Int.*, **208**, 38–43, doi: /10.1016/j.quaint.2009.02.018.

Zhang, K. X., R. Wang, C. C. Shen, et al., 2010a: Temporal and spatial characteristics of the urban heat island during rapid urbanization in Shanghai, China. *Trans. Tianjin Uni.*, **169**, 101–112, doi: /10.1007/s10661-009-1154-8.

Zhang, N., Z. Q. Gao, X. M. Wang, et al., 2010b: Modeling the impact of urbanization on the local and regional climate in Yangtze River Delta, China. *Trans. Tianjin Uni.*, **102**, 331–342, doi: /10.1007/s00704-010-0263-1.

Zhang, L., Xue, J., Wang, W., et al., 2014: Comparative analysis of extreme high temperature weather in the summers of 2013 and 2003. *Atmos. Oceanic Sci. Lett.*, **7**, 132–136, doi: /10.3878/j.issn.1674-2834.13.0073.

Zhang, H. S., X. Y. Zhang, Q. H. Li, et al., 2020: Research progress on estimation of the atmospheric boundary layer height. *J. Meteor. Res.*, **34**, 482–498, doi: 10.1007/s13351-020-9910-3.

Zhang, P. F., G. Y. Ren, Y. Qin, et al., 2021: Urbanization effects on estimates of global trends in mean and extreme air temperature, *J. Climate*, **34**, 1923-1945. doi: /10.1175/JCLI-D-20-0389.1.

Zhai, P. M., and X. H. Pan, 2003: Trends in temperature extremes during 1951–1999 in China. *Geophys. Res. Lett.*, **30**, 169–172, doi: /10.1029/2003gl018004.

Zhong, S., Y. Qiang, C. Zhao, et al., 2017: Urbanization-induced urban heat island and aerosol effects on climate extremes in the Yangtze River Delta region of China. *Atmos. Chem. Phys.*, **17**, 1–57, doi: /10.5194/acp-2016-953.

Zittis, G., P. Hadjinicolaou, M. Fnais, et al., 2015: Projected changes in heat wave characteristics in the eastern Mediterranean and the Middle East. *Reg. Environ.*, **16**, 1863–1876, doi: /10.1007/s10113-014-0753-2.